2.2 Blocking of the Wind by Terrain

Throughout Section 2.1 we considered various atmospheric phenomena that arise due to air flowing over mountains. In this section we will investigate phenomena that result from the blocking of wind by terrain.

2.2.1 Over or Around?

Consider an air parcel approaching a mountain. Will it go over or around the mountain? What factors determine the parcel's path?

The air parcel's path depends on several factors:

- the height of the parcel relative to the height of the mountain
- the slope and dimensions (height/width) of the mountain
- the static stability
- the strength of the upstream horizontal winds directed at the mountain

Some general scenarios when a parcel is most likely to go around rather than over a mountain include

- there is increased stratification
- the speed of an approaching parcel decreases
- the distance that must be climbed by a parcel increases

Perhaps the intuitive method to assess the potential for blocking is to compare the kinetic energy of an approaching parcel to the work that must be done to overcome stratification and lift the parcel over the barrier. This method, however, neglects pressure perturbations. We previously saw that pressure perturbations were very important to flow over a mountain, especially when considering downslope wind events. To properly account for the effects of pressure perturbations we will make use of a Bernoulli equation.

Consider a streamline in steady flow that passes over a barrier (Fig. 1). Far upstream ($x = -\infty$), the streamline is located at some height z_0. Near the barrier, the streamline is displaced upward some distance δ, such

that its new height is $z_0 + \delta$. Here, we assume that parcel motions are dry adiabatic, meaning that $\theta = \theta_0$ along a streamline.

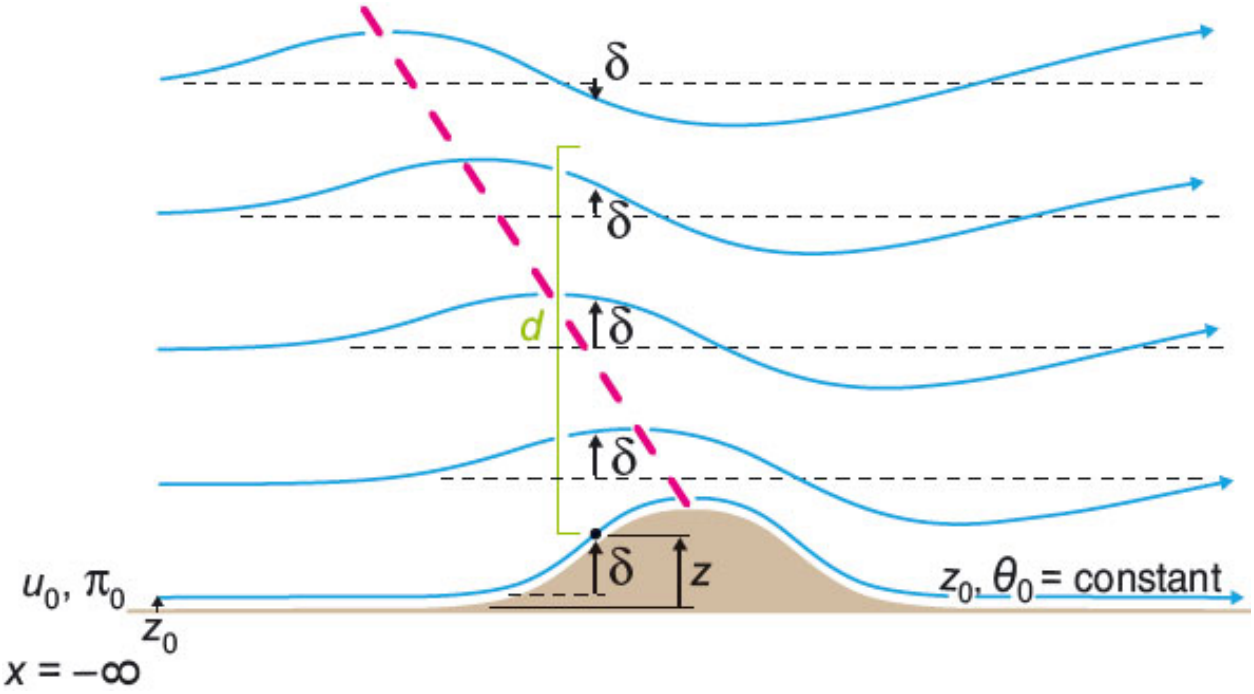

Figure 1: A schematic illustration of streamlines (blue; coincident with isentropes for inviscid, dry adiabatic motion), passing over a mountain, along which the Bernoulli equation applies. [From Markowski and Richardson]

For a steady flow, the Bernoulli equation (see Chapter 2 in Markowski and Richardson) is given by

$$\Pi + \frac{u^2}{2c_p\theta_0} + \frac{gz}{c_p\theta_0} = \text{constant}, \tag{1}$$

where $\Pi = (p/p_0)^{R/c_p}$ is non-dimensional pressure (the so-called Exner function) and c_p is the specific heat of air at constant pressure. Far upstream, this equation becomes

$$\Pi_0 + \frac{u_0^2}{2c_p\theta_0} + \frac{gz_0}{c_p\theta_0} = \text{constant}, \tag{2}$$

where Π_0 and u_0 are the respective upstream values for the non-dimensional pressure and barrier-normal wind component where the streamline is at height z_0.

We now define the non-dimensional pressure such that

$$\Pi^{'} = \Pi(z) - \overline{\Pi}(z),$$

where $\Pi(z)$ is the value at some height z and $\overline{\Pi}(z)$ is the far upstream value at the same level.

Using this definition, we can combine Eqs. (1) and (2) as

$$\Pi^{'} + \overline{\Pi} + \frac{u^2}{2c_p\theta_0} + \frac{gz}{c_p\theta_0} = \Pi_0 + \frac{u_0^2}{2c_p\theta_0} + \frac{gz_0}{c_p\theta_0} \, . \tag{3}$$

Assuming hydrostatic upstream conditions, you can show that $-\rho^{-1}\partial p/\partial z = -c_p\theta\partial\Pi/\partial z$, which leads to

$$\overline{\Pi}(z) = \Pi_0 - \frac{g}{c_p}\int_{z_0}^{z} \overline{\theta}(z)^{-1} dz \, , \tag{4}$$

where $\overline{\theta}(z)$ is the upstream profile of potential temperature. Now we assume that the upstream stratification is independent of height, such that

$$\overline{\theta}(z) = \theta_0 + \frac{\partial\overline{\theta}}{\partial z}(z - z_0) = \theta_0\left(1 + \frac{N^2\delta}{g}\right) \, , \tag{5}$$

where $\delta = z - z_0$ and $N^2 = (g/\theta_0)\partial\overline{\theta}/\partial z$ is the upstream Brunt-Väisälä frequency. Here, we can assume $(1 + N^2\delta/g)^{-1} \approx (1 - N^2 g/\delta)$. We plug the resulting expression into Eq. (4), which yields

$$\overline{\Pi}(z) = \Pi_0 - \frac{g\delta}{c_p\theta_0} + \frac{N^2\delta^2}{2c_p\theta_0} \, . \tag{6}$$

Next, we substitute Eq. (6) into Eq. (3):

$$u^2 = u_0^2 - 2c_p\theta_0\Pi^{'} - N^2\delta^2 \, . \tag{7}$$

If $\Pi^{'} = 0$, then

$$u^2 = u_0^2 - N^2\delta^2 \, . \tag{8}$$

For stably stratified conditions ($N^2 > 0$), the air will slow down as it ascends the mountain ($u \downarrow$ when $\delta \uparrow$). Equation (8) shows that the flow will stagnate ($u \to 0$) when δ reaches a critical level, defined as

$$\delta_{max} = \frac{u_0}{N} \, . \tag{9}$$

In other words, air flowing along the surface is unable to pass over terrain taller than u_0/N, regardless of the terrain shape. The so-called *dividing streamline* is the streamline that separates flow passing around the sides of the obstacle from flow passing over the obstacle.

Eqs. (8) and (9) form the basis for the popular forecasting criterion for blocking in terms of the *mountain Froude number*, $\mathrm{F_{rm}} = u_0/(Nh_m) = \delta_{max}/h_m$, where h_m is the mountain height. Thus, at least part of the flow will be blocked when $\mathrm{F_{rm}} < 1$ ($h_m > \delta_{max}$).

However, observations and simulations reveal that $\mathrm{F_{rm}}$ is too simplistic to properly describe whether or not terrain will block the flow. Reasons include:

- Eq. (8) predicts that the minimum wind speeds exist at the crest of the mountain. Observations, however, show that the minimum wind speeds often occur halfway up the windward side of the mountain.
- Observations and simulations both indicate that terrain slope and aspect ratio (crosswise divided by streamwise) are critical factors affecting the tendency for blocking. For instance, blocking is more likely as the slope and aspect ratio of the terrain increase.

The reason for these discrepancies is that pressure perturbations are very important (if not the dominant factor) in determining an air parcel's acceleration as it approaches a barrier. Recall that we previously assumed that $\Pi^{'} = 0$. In order to more physically determine whether the flow will be blocked, we must construct an expression for u that considers pressure perturbations.

If the barrier's slope is not too steep, then dw/dt is small enough that the pressure perturbation can be obtained by integrating the hydrostatic equation:

$$\Pi^{'} = -\frac{g}{c_p}\int_z^\infty \frac{\theta^{'}}{\theta_0^2}dz = \frac{N^2}{c_p\theta_0}\int_z^\infty \delta dz\,, \tag{10}$$

where $\theta^{'} = \theta_0 - \overline{\theta}(z)$ is the potential temperature perturbation, which is proportional to $\delta(x, y, z)$, and $\Pi^{'} = \Pi_h^{'}$ is the non-dimensional hydrostatic pressure perturbation.

Clearly, Eq. (10) is problematic since the lower limit of integration changes as the height of the streamline changes. We attempt to alleviate this issue by writing δ in terms of (x, y, z_0), where $z_0(\theta)$ is the upstream height of each isentrope. Note that since $z = z_0 + \delta$, then $dz = dz_0 + d\delta$. This relationship is used to rewrite Eq. (10) as

$$\Pi^{'} = \frac{N^2}{c_p\theta_0}\left(\int_{z_0}^\infty \delta dz_0 + \int_\delta^0 \delta d\delta\right)\,, \tag{11}$$

where we have assumed that $\delta \to 0$ as $z_0 \to \infty$.

We now define the integral of displacement I_δ as

$$I_\delta = \int_{z_0}^\infty \delta dz_0\,, \tag{12}$$

then Eq. (11) can be written as

$$\Pi^{'} = \frac{N^2}{c_p\theta_0}\left(I_\delta + \frac{\delta^2}{2}\right)\,, \tag{13}$$

and Eq. (7) becomes

$$u^2 = u_o^2 - 2N^2 I_\delta\,. \tag{14}$$

Equation (14) is a more physically relevant diagnostic tool that relates wind speed to the vertical displacement field. Not only is it useful for assessing low-level blocking, it can be applied to upper-level streamlines to predict stagnation (which leads to wave breaking). The meaningful distinction between Eqs. (7) and (14) is that the latter controls wind speed by the integral of vertical displacement above a point, while the former only considers local displacement.

The greater the integrated upward displacements, the greater the negative buoyancy in the overlying column, and the greater the resulting pressure perturbation. Stagnation occurs where

$$I_\delta = \frac{u_0^2}{2N^2} \,. \tag{15}$$

At a given height, the slowest flow occurs where there is a local maximum of I_δ. At such a maximum,

$$\frac{\partial I_\delta}{\partial z_0} = \frac{\partial}{\partial z_0} \int_{z_0}^{\infty} \delta dz_0 = 0 \,, \tag{16}$$

thus, $\delta = 0$ where wind speed is a minimum.

In order to predict the critical mountain height for which approaching flow will be blocked, one must estimate I_δ. This is very difficult. Historically, this was accomplished through linear theory.

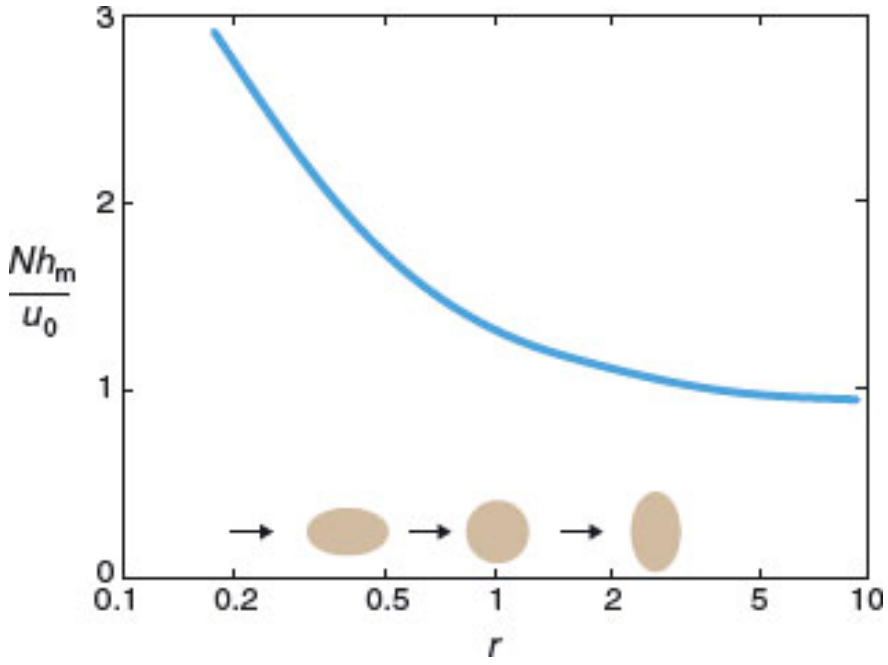

Figure 2: The non-dimensional mountain height where stagnation begins, as a function of the aspect ratio of the mountain (crosswise dimension divided by streamwise dimension) for an air parcel moving along the surface. [From Markowski and Richardson]

There are a couple of immediate takeaways from this work by Smith (1990)

- The tendency for blocking increases as the aspect ratio increases for a given non-dimensional mountain height.
- Stagnation begins at a non-dimensional height of ~ 1 for mountains with large aspect ratios. Therefore, $\mathrm{F_{rm}}$ is a reasonably good predictor for blocking for mountains with those particular geometries.

In practice, $\mathrm{F_{rm}}$ is computed using upstream surface winds and the vertically-averaged N (over the depth of the mountain) to improve its physical utility.

A second non-dimensional number used to assess blocking potential is the *Burger number*, given by

$$\mathrm{B_u} = \frac{\mathrm{R_o}}{\mathrm{F_{rm}}} = \frac{N h_m}{L_m f} \,, \tag{17}$$

where L_m is the streamwise half-width of the mountain, f is the Coriolis parameter, and h_m/L_m is the slope of the mountain. Thus, the Burger number considers the effects of both the steepness of the terrain and the effects of rotation. Recall that Eq. (10) assumes that the barrier is not steeply sloped and ignores the Coriolis force. Blocking can occur when $\mathrm{B_u} > 1$, even when $\mathrm{F_{rm}} > 1$. This scenario represents terrain that is considered *hydrodynamically steep*. As the flow is forced up the steep terrain, a strong adverse pressure gradient force is generated.

2.2.2 Cold-Air Damming

In the eastern United States, northerly surges of cold air down the east side of the Appalachian Mountains are commonly observed in winter on the south side of a surface anticyclone, where winds having an easterly geostrophic wind component are directed from offshore toward the mountains, and are blocked and deflected southward by the mountains. This type of orographically trapped cold-air surge is locally referred to as *cold-air damming*. Cold-air damming occurs in virtually every significant East Coast freezing and frozen precipitation event. The phenomena has also been observed over the Front Range of the Rocky Mountains.

In most cold-air damming cases, the lower atmosphere satisfies

$$h_m > \frac{u}{N} \rightarrow \mathrm{F_{rm}} < 1 \,, \tag{18}$$

where u is the barrier-normal wind component and N is the vertically (over the depth of the barrier) averaged Brunt-Väisälä frequency. If the flow is blocked over a significant depth, $\mathrm{F_{rm}}$ is significantly less than one.

The obvious takeaway from Eq. (18) is that these trapped surges are favored in strongly stable environments. Upwind clouds, especially those that precipitate into a dry boundary layer, further act to enhance the potential for damming.

Consider a low-level flow approaching a north-south mountain barrier from the east (see Fig. 3 for a conceptual model). Winds are deflected southward, resulting in a large southward ageostrophic wind component east of the barrier. A ridge of high pressure builds southward as a hydrostatic consequence of the trapped cold air. The width of this pressure ridge is approximated by the *Rossby radius of deformation*,

$$L_R = \frac{Nh}{f} \,, \tag{19}$$

where f is the Coriolis parameter, h is the scale height of the flow that is perturbed by the terrain, and N is some representative value over h. When $\mathrm{F_{rm}} < 1$, an appropriate scale height is $h = h_I = u/N$, where h_I is known as the *inertial height scale*. In this case, the previous equation becomes

$$L_R = \frac{u}{f} = L_{Rm}\mathrm{F_{rm}} \,, \tag{20}$$

where $L_{Rm} = Nh_m/f$ is the so-called *mountain Rossby radius*.

In the case of a layer of warm air subsiding over the cold air, separated by a strong inversion, the system approaches a two-layer system. In this case,

$$L_R = \frac{\sqrt{g'H}}{f} \,, \tag{21}$$

where $g^{'} = g\Delta\theta/\overline{\theta}$ is reduced gravity, H is the depth of the cold layer, $\overline{\theta}$ is the mean potential temperature of the cold layer, and $\Delta\theta$ is the potential temperature gradient across the inversion.

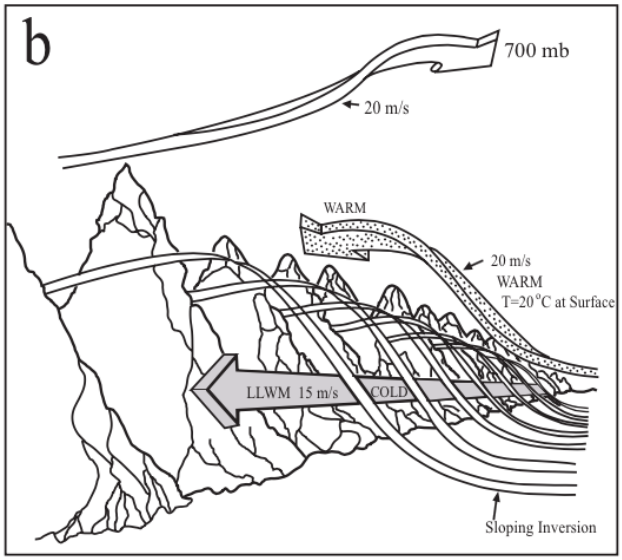

Figure 3: Conceptual model of a mature cold-air damming event. LLWM stands for low-level wind maximum. (Adapted after Bell and Bosart 1988)

In terms of deflection, again consider an air parcel approaching a north-south mountain barrier from the east (Fig. 4). An example of this setup is an episode of cold-air damming east of the Appalachian Mountains when an anticyclone is positioned to the north of the parcel.

- Far upstream the parcel experiences no net acceleration owing to a balance among the pressure gradient, Coriolis, and friction forces
- The parcel decelerates once it begins ascending
- This deceleration is associated with a weakening of the northward-directed Coriolis force, resulting in a southward deflection by the large-scale pressure gradient force
- Once air has been diverted southward, the Coriolis force keeps the cold air trapped against the mountains (Fig. 5)
- Farther upstream within the cold-air mass (where northerly winds are approximately steady and blowing roughly along the elevation contours) the pressure gradient force is directed downslope and is in approximate balance with the upslope-pointing Coriolis force and friction forces.
- If the atmosphere is stably stratified, the parcel decelerates as it nears and ascends the mountain range.
- If the pressure gradient force is the same near the mountain range as it is a large distance from the mountains, then the upstream balance among the pressure gradient, Coriolis, and friction forces cannot be maintained as higher terrain is encountered.
- The parcel experiences a net acceleration in the direction of the pressure gradient force.
- In many cold-air surge cases, the deflection of air by the terrain produces a barrier jet on the upslope side of the barrier.
- Barrier jets can attain wind speeds of $15\text{-}30\ \mathrm{ms}^{-1}$ and are usually centered at an altitude roughly half the height of the mountain crest.

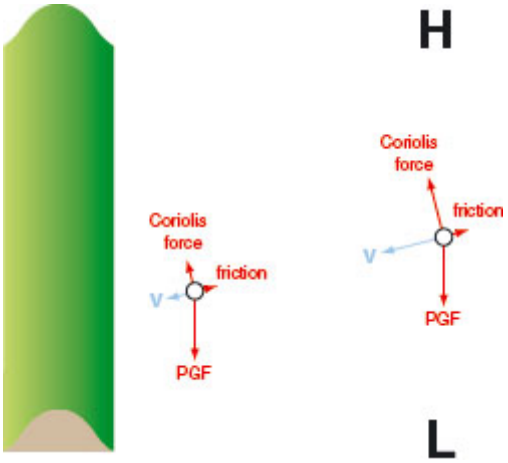

Figure 4: Force diagrams for an air parcel approaching a northern hemisphere mountain range in a situation with $\mathrm{F_{rm}} < 1$. [From Markowski and Richardson]

The approximate scale of the velocity increase in the direction parallel to the coast or mountain range is

$$\Delta v \approx \frac{N^2 h_I^2}{f L_{Rm}} = \frac{u^2}{f L_{Rm}} \,, \tag{22}$$

where v is the barrier-parallel wind component. The strongest barrier jets are therefore observed when there is a strong mountain-normal wind (u) and small mountain Rossby radius L_{Rm}, and thus small N and h_m, but not so small (nor u so large) that $\mathrm{F_{rm}} > 1$.

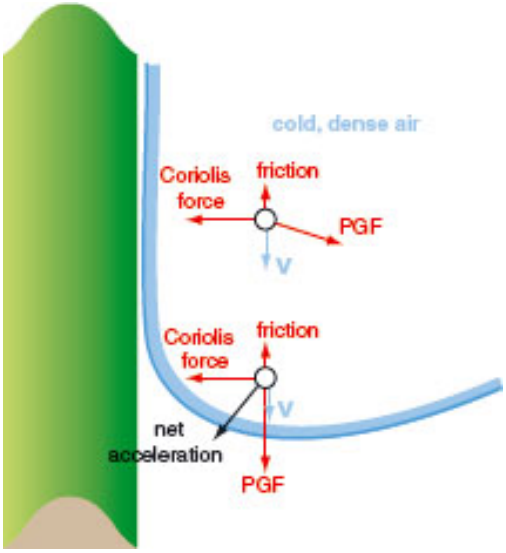

Figure 5: Schematic illustration of the damming of cold air against a mountain range in the northern hemisphere. [From Markowski and Richardson]

2.2.3 Lee Vortices

Counter-rotating vortices are commonly observed in the lee of an isolated terrain obstacle when the flow is strongly stratified and forced to pass around the obstacle. On some occasions a single pair of oppositely signed vertical vorticity extrema is observed in the wake of the obstacle (Fig. 6). When the wake flow in which the lee vortices are embedded becomes unstable, the vortices tend to shed downstream and form a *von Kármán vortex street* (Fig. 7). A von Kármán vortex street is a repeating pattern of alternate and swirling vortices along the center line of the wake flow, and is named after the fluid dynamicist, Theodore von Kármán. This process is also known as vortex shedding.

You might assume that all wake vortices form as a result of the separation of a viscous boundary layer from an obstacle. However, numerical simulations with no surface drag also contain wake vortices, despite frictional stress being entirely absent at the lower boundary. These simulated vortices actually decrease in intensity when surface friction is added. This variety of wake vortices, at least in numerical simulations, is confined to a range of $\mathrm{F_{rm}}$ between 0.1 and 0.5, which is fairly typical of cases in which wake vortices are observed in the real atmosphere. In the case of wake vortices that form as a result of a purely inviscid mechanism, baroclinic vorticity generation is key (read pages 351-355 in Markowski and Richardson for further details).

For $\mathrm{F_{rm}}$ outside of the range of 0.1-0.5, wake vortices are not observed to form as a result of purely inviscid processes, at least not in numerical simulations. When wake vortices are observed outside of this range of $\mathrm{F_{rm}}$, it is likely that the separation of the viscous boundary layer from the obstacle has played the dominant role in their formation.

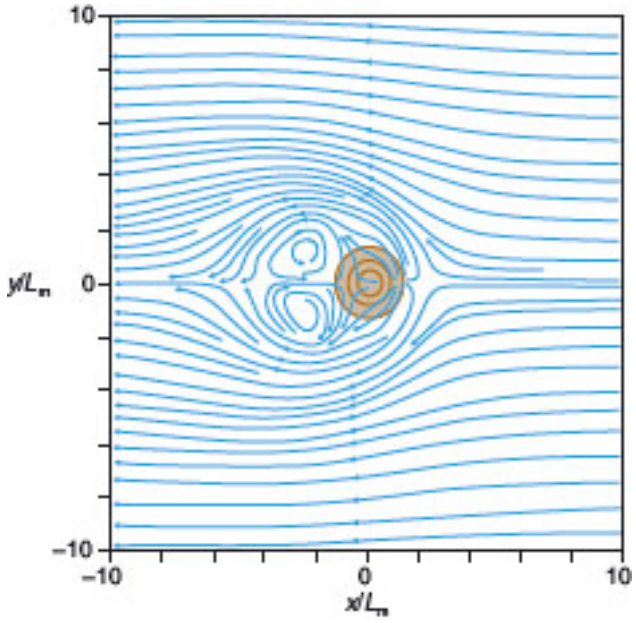

Figure 6: Example of a pair of counter-rotating vortices in the wake of an isolated mountain peak in a numerical simulation. [From Markowski and Richardson]

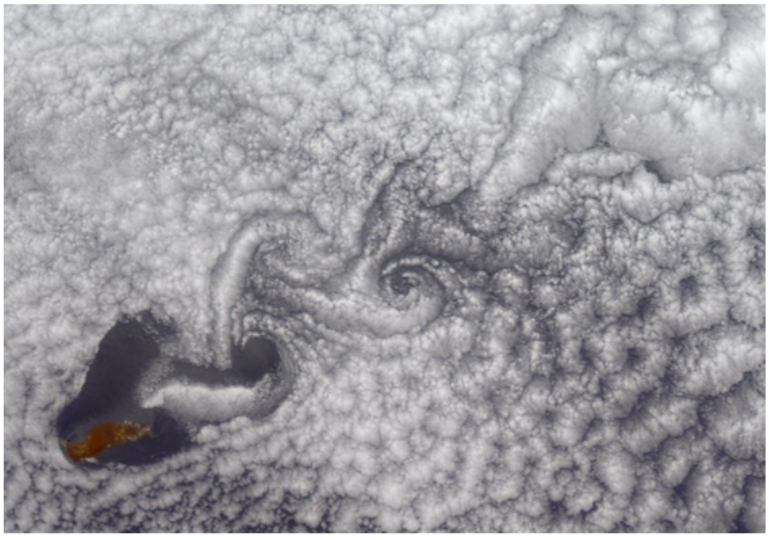

Figure 7: A von Kármán vortex street that formed to the lee of the Guadalupe Island, off the coast of Mexico's Baja Peninsula, revealed by MISR images from June 11, 2000 detected by NASA satellite Terra. (credit: Visible Earth, NASA)

2.2.4 Gap Flows

When a low-level wind passes through a gap in a mountain barrier or a channel between two mountain ranges, it can significantly strengthen due to the acceleration associated with the along-gap pressure gradient force. The significant pressure gradient is often established by (a) the geostrophically balanced pressure gradient associated with the synoptic-scale flow and/or (b) the low-level temperature differences in the air masses on each side of the mountains.

Gap flows occurring in the atmosphere are also known as mountain-gap winds, jet-effect winds, or canyon winds. Gap flows perhaps most often occur in conjunction with cold-air surges, when significant cross-barrier temperature differences and cross-barrier winds may both be present.

Gap flows are found in many different places in the world. Examples include the Columbia River Gorge and the Strait of Juan de Fuca in the northwestern United States (Fig. 8), the Rhine Valley of the Alps, the Sierra Nevada in Independence, California, and the lee side of the Rockies in Boulder, Colorado.

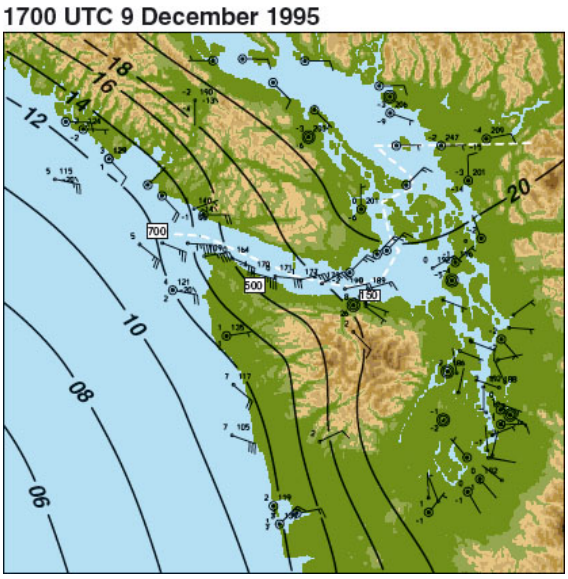

Figure 8: Surface analysis from 1700 UTC 9 Dec 1995 during a gap flow event in the Strait of Juan de Fuca. The contour interval for sea level pressure is 2mb. [From Markowski and Richardson]

Based on $\mathrm{F_{rm}}$, three gap-flow regimes can be identified (see Fig. 9):

- *linear regime* (large $\mathrm{F_{rm}}$): insignificant enhancement of the gap flow;
- *mountain wave regime* (mid-range $\mathrm{F_{rm}}$): large increases in the mass flux and wind speed within the exit region due to downward transport of mountain wave momentum above the lee slopes, and where the highest wind occurs near the exit region of the gap
- *upstream-blocking regime* (small $\mathrm{F_{rm}}$): the largest increase in the along-gap mass flux occurs in the entrance region due to lateral convergence

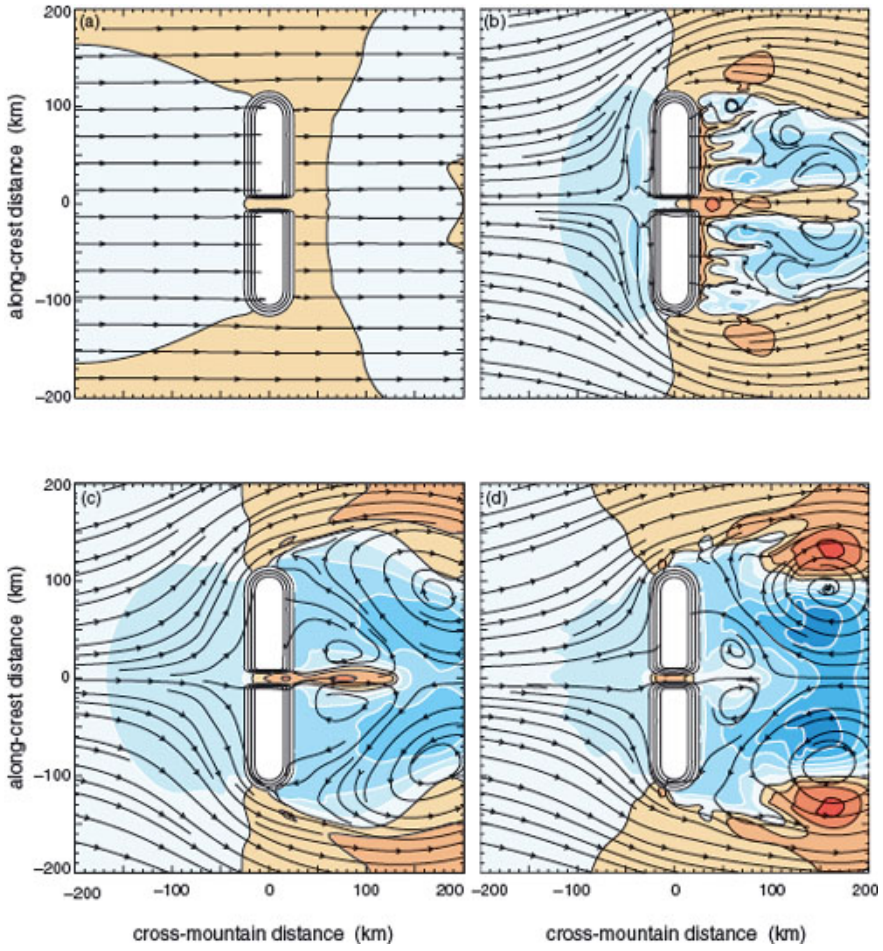

Figure 9: Idealized numerical simulation of westerly winds encountering a ridge with a gap when the F_{rm} is equal to (a) 4.0, (b) 0.7, (c) 0.4, and (d) 0.2. Horizontal streamlines and normalized perturbation velocity ((u-U)/U, where u is the zonal wind speed and U is the zonal wind speed far upstream; shaded contours) at z = 300 m are shown. The contour interval is 0.5; warm (cold) color shading corresponds to positive (negative) values. Terrain contours are every 300 m. Notice how (a) and (b)-(d) represent flow-over and flow-around regimes, respectively, as would be expected from the differences in F_{rm}.[From Markowski and Richardson]

Gap flows are also influenced by frictional effects, which imply that:

- the flow is much slower
- the flow accelerates through the gap and upper part of the mountain slope
- the gap jet extends far downstream
- the slope flow separates, but not the gap flow
- the highest winds occur along the gap